

harmonicity. Note that this is a conservative statement, because our energy difference between the bridged and the Y-shaped structures is somewhat smaller than the best theoretical estimate (6).

The qualitative features of the ϕ_{21} - ϕ_{13} distribution at 3000 K (Fig. 2F) resemble those obtained for the ground state (Fig. 2D). However, the magnitude of the out-of-plane trans distortion has increased considerably at 3000 K to $\Delta\gamma \approx \pm 0.23 \text{ \AA}$ and $\Delta\theta \approx 23^\circ$. This is consistent with the qualitative change of the E_1 - E_2 projection with increasing temperature: The maximum at $(S, E_1, E_2) \approx (0, 0, \sqrt{2})$ is shifted to about $(0, 0, 1.33)$ at 3000 K (Fig. 2E). This corresponds neither to the bridged nor to the Y-shaped structure, but rather to a distorted one with $(\theta_1, \theta_2, \theta_3) \approx (90^\circ, 20^\circ, 160^\circ)$. Ignoring the important differences between our real space and the velocity space of CEI, which is smeared by multiple scattering, this is very close to the values $(90^\circ, 30^\circ, 150^\circ)$ inferred from CEI (2). In addition, the features of Fig. 2E, with the six peaks connected by saddle points at about half the peak height and the (S, E_1, E_2) peaks shifted away from $(0, 0, \pm\sqrt{2})$, resemble those obtained from CEI (2). Thus, we observe only at quite high temperatures the behavior attributed to the ground state of $C_2H_3^+$ by CEI (2). Again, note that for a quantitative comparison of our real space distributions with CEI data reported only in velocity space, a simulation (11, 13) of the Coulomb scattering process itself has to be carried out.

We summarize our main points pictorially by superimposing in Fig. 3 representative configurations obtained from the trajectories of $C_2H_3^+$. The resulting smearing is induced either by thermal or by quantum fluctuations of the molecular structure. As expected, the classical distribution at 5 K (Fig. 3A) is nearly indistinguishable from the planar bridged minimum structure. In the quantum ground state (Fig. 3B) the protons are mainly localized around the bridged configuration in Fig. 3A and exchange sites through tunneling. Thus, the quantum ground-state structure of $C_2H_3^+$ is best described as a quasi-planar bridged structure broadened significantly by anisotropic delocalization of the protons due to zero point motion. Rotational excitations at higher temperatures lead only to a broad distribution of nonplanar structures, including bridged and Y-shaped ones (Fig. 3C).

How does the scenario predicted by ab initio simulations compare with the CEI data? As demonstrated, the quantum ground-state structure is clearly different from what was deduced from CEI (2). We obtain, however, good agreement with the CEI data at high temperatures. This strongly suggests that CEI (2) did not probe the quantum ground state of the floppy mole-

cule $C_2H_3^+$, but an ensemble of ro-vibrationally excited molecules. This aspect calls for further clarifications in view of the extraordinary prospects of CEI to probe non-rigid molecular structures (11).

REFERENCES AND NOTES

- R. J. Saykally, *Science* **239**, 157 (1988).
- Z. Vager, D. Zajfman, T. Graber, E. P. Kanter, *Phys. Rev. Lett.* **71**, 4319 (1993).
- M. W. Crofton, M.-F. Jagod, B. D. Rehfuss, T. Oka, *J. Chem. Phys.* **91**, 5139 (1989); see also T. Oka, *Philos. Trans. R. Soc. London Ser. A* **324**, 81 (1988).
- M. Bogey, M. Cordonnier, C. Demuyneck, J. L. Desbordes, *Astrophys. J.* **399**, L103 (1992); in *Structures and Conformations of Non-Rigid Molecules*, J. Laane, M. Dakkouri, B. van der Veken, H. Oberhammer, Eds. (Kluwer, Dordrecht, Netherlands, 1993), pp. 303-323.
- M. Bogey *et al.*, *Can. J. Phys.* **72**, 967 (1994); for a review, see C. Demuyneck, *J. Mol. Spectrosc.* **168**, 215 (1994).
- R. Lindh, J. E. Rice, T. J. Lee, *J. Chem. Phys.* **94**, 8008 (1991).
- W. Klopffer and W. Kutzelnigg, *J. Phys. Chem.* **94**, 5625 (1990).
- C. Liang, T. P. Hamilton, H. F. Schaefer III, *J. Chem. Phys.* **92**, 3653 (1990).
- J. S. Tse, D. D. Klug, K. Laasonen, *Phys. Rev. Lett.* **74**, 876 (1995).
- G. A. Olah, G. K. S. Prakash, R. E. Williams, L. D. Field, K. Wade, *Hypercarbon Chemistry* (Wiley, New York, 1987).
- Z. Vager, R. Naaman, E. P. Kanter, *Science* **244**, 426 (1989).
- J. Berkowitz, C. A. Mayhew, B. Rušćić, *J. Chem. Phys.* **88**, 7396 (1988).
- D. Zajfman *et al.*, *ibid.* **94**, 6377 (1991); D. Zajfman, T. Graber, E. P. Kanter, Z. Vager, *Phys. Rev. A* **46**, 194 (1992).
- R. Car and M. Parrinello, *Phys. Rev. Lett.* **55**, 2471 (1985).
- For reviews, see R. O. Jones and O. Gunnarsson, *Rev. Mod. Phys.* **61**, 689 (1989); D. K. Remler and P. A. Madden, *Mol. Phys.* **70**, 921 (1990).
- D. W. Boo, Z. F. Liu, A. G. Suits, J. S. Tse, Y. T. Lee, *Science* **269**, 57 (1995).
- D. Marx and M. Parrinello, *Z. Phys. B (Rapid note)* **95**, 143 (1994).
- _____, *Nature* **375**, 216 (1995).
- D. M. Ceperley, *Rev. Mod. Phys.* **67**, 279 (1995).
- D. Chandler, in *Liquids, Freezing, and Glass Transition*, J. P. Hansen, D. Levesque, J. Zinn-Justin, Eds. (Elsevier, Amsterdam, 1991), pp. 193-285.
- For the bridged structure, $r_{CC} = 1.233 \text{ \AA}$, $r_{CH1} = 1.304 \text{ \AA}$, $r_{CH2} = 1.101 \text{ \AA}$ (where r_{ij} is the distance between the i and j atoms), and the angle formed by H1-C-H2 (\angle_{H1CH2}) is 117.8° ; here, H1 and H2 denote the bridging and terminal protons, respectively. For the Y-shaped structure, $r_{CC} = 1.255 \text{ \AA}$, $r_{CH1} = 1.104 \text{ \AA}$, $r_{CH2} = 1.123 \text{ \AA}$, and $\angle_{H1CH2} = 115.8^\circ$; here, H1 denotes the proton that forms the linear H1-C-C bond, and H2 denotes the other two equivalent protons. For notation and structures, see also (8).
- E. P. Kanter, Z. Vager, G. Both, D. Zajfman, *J. Chem. Phys.* **85**, 7487 (1986).
- A search for the maximum directly in $(S, E_1, E_2, \phi_{21}, \phi_{13})$ real space for the quantum nuclei at 5 K yielded approximately $(0, 0, 1.414, 100^\circ, 120^\circ)$, and the other equivalent maxima are related by symmetry. The uncertainty of the ϕ_i coordinates is estimated to amount to at least $\pm 10^\circ$.
- For the average structure with rms fluctuations, $r_{CC} = 1.235 \pm 0.013 \text{ \AA}$, $r_{CH1} = 1.320 \pm 0.090 \text{ \AA}$, $r_{CH2} = 1.103 \pm 0.016 \text{ \AA}$, and $\angle_{H1CH2} = 118.1 \pm 5^\circ$; for the most probable structure, $r_{CC} = 1.234 \text{ \AA}$, $r_{CH1} = 1.290 \text{ \AA}$, $r_{CH2} = 1.104 \text{ \AA}$, and $\angle_{H1CH2} = 117.7^\circ$. Both structures were obtained with quantum nuclei at 5 K with the notation defined in (27).
- A substantial part of the computations was carried out on the SP1 at the IBM Thomas J. Watson Research Center.

8 August 1995; accepted 27 October 1995

Controlled Room-Temperature Positioning of Individual Molecules: Molecular Flexure and Motion

T. A. Jung, R. R. Schlittler, J. K. Gimzewski, H. Tang, C. Joachim

Two-dimensional positioning of intact individual molecules was achieved at room temperature by a controlled lateral "pushing" action of the tip of a scanning tunneling microscope. To facilitate this process, four bulky hydrocarbon groups were attached to a rigid molecule. These groups maintained sufficiently strong interactions with the surface to prevent thermally activated diffusional motion, but nevertheless allowed controllable translation. Simulations demonstrated the crucial role of flexure during the positioning process. These results outline the key role of molecular mechanics in the engineering of predefined properties on a molecular scale.

Nanofabrication combines physical and chemical processes to assemble structures on the molecular scale. Important elements of engineering at this level, such as the con-

trolled assembly of molecular arrays (supramolecular chemistry), require the positioning and interlocking of intact molecules without disruption of their internal atomic structure. Scanned probe microscopy (SPM) (1) combines the capability for manipulation of individual atoms and molecules with high-resolution imaging for determination of structure and orientation. Typically, manipulation has involved the breaking of atomic bonds through the use of voltage pulses,

T. A. Jung, R. R. Schlittler, J. K. Gimzewski, IBM Research Division, Zurich Research Laboratory, CH-8803 Rüschlikon, Switzerland.

H. Tang and C. Joachim, Centre d'Elaboration de Matériaux et d'Etudes Structurales-Centre National de la Recherche Scientifique, 29 rue J. Marvig, Post Office Box 4347, F-31055 Toulouse Cedex, France.

electric fields, or mechanical contact (1). Only at low temperatures has the precise repositioning of individual molecules such as

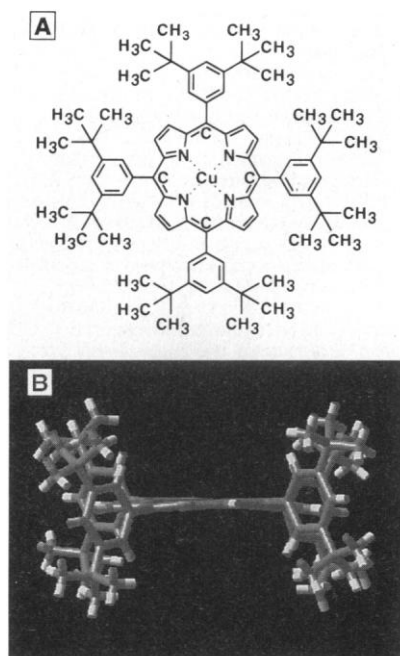


Fig. 1. (A) Structure and (B) conformation of Cu-TBP-porphyrin. The DTP substituents are oriented perpendicular to the porphyrin plane. Steric repulsion of hydrogen atoms with the porphyrin and phenyl groups hinders rotation of the DTP substituent. Consequently, the porphyrin-phenyl bond of TBP-porphyrin is a single (σ) bond that does not participate in the conjugated electron system, owing to the weak overlap of the π levels. This is confirmed by the variation of bond angles reported in x-ray data (10) and by our STM data resolving different molecular conformations, depending on substrate and adsorption site.

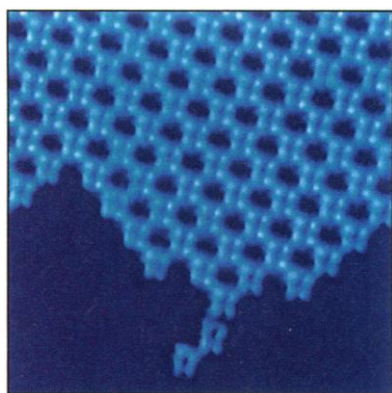


Fig. 2. STM topograph of Cu-TBP-porphyrin sublimated at a base pressure below 10^{-10} mbar onto Cu(100) samples previously prepared by cycles of Ne^+ sputtering and annealing at ~ 700 K. After further annealing for 3 min at 550 K, islands with a $\sqrt{58} \times \sqrt{58}$ superstructure nucleate. Under imaging conditions ($U \sim 2200$ V and $I \sim 80$ pA), each individual molecule is imaged as four bright lobes corresponding to the four DTP substituents. Image area: 21 nm by 21 nm.

CO been demonstrated (2) without breaking intramolecular bonds. The use of low temperatures permits weakly bonded molecules to be repositioned with the scanning tunneling microscope (STM) tip while limiting thermal motion. However, at room temperature, the level of thermal energy [kT (k , Boltzmann's constant, T , temperature)] necessitates strong bonding of an isolated molecule to the substrate to prevent uncontrolled diffusion. This bonding must not be so strong that it hinders controlled movement of the molecule by the tip. The choice of the molecule is therefore crucial for the simultaneous realization of molecular stability and ease of positioning.

Here we demonstrate room-temperature positioning of porphyrin-based molecules into stable predefined patterns without disruption of internal molecular

bonds. Molecular mechanic simulations reveal the role of molecular flexure in the translation process. By evaluating a range of different molecular systems, we have found that a specific copper porphyrin molecule meets the criteria for positioning as outlined above. The molecule is Cu-tetra-(3,5 di-tertiary-butyl-phenyl)-porphyrin (Cu-TBP-porphyrin) (Fig. 1A) with four di-tertiary butyl phenyl (DTP) substituents (legs). These four legs are rotated out of the plane of the porphyrin ring because of a steric repulsion effect (Fig. 1B). Consequently, the saturated *t*-butyl groups attached to the legs dominate the interactions between the molecule and the surface. A degree of rotation of the phenyl group with respect to the porphyrin as well as rotation of the *t*-butyl groups is possible. The *t*-butyl groups interact

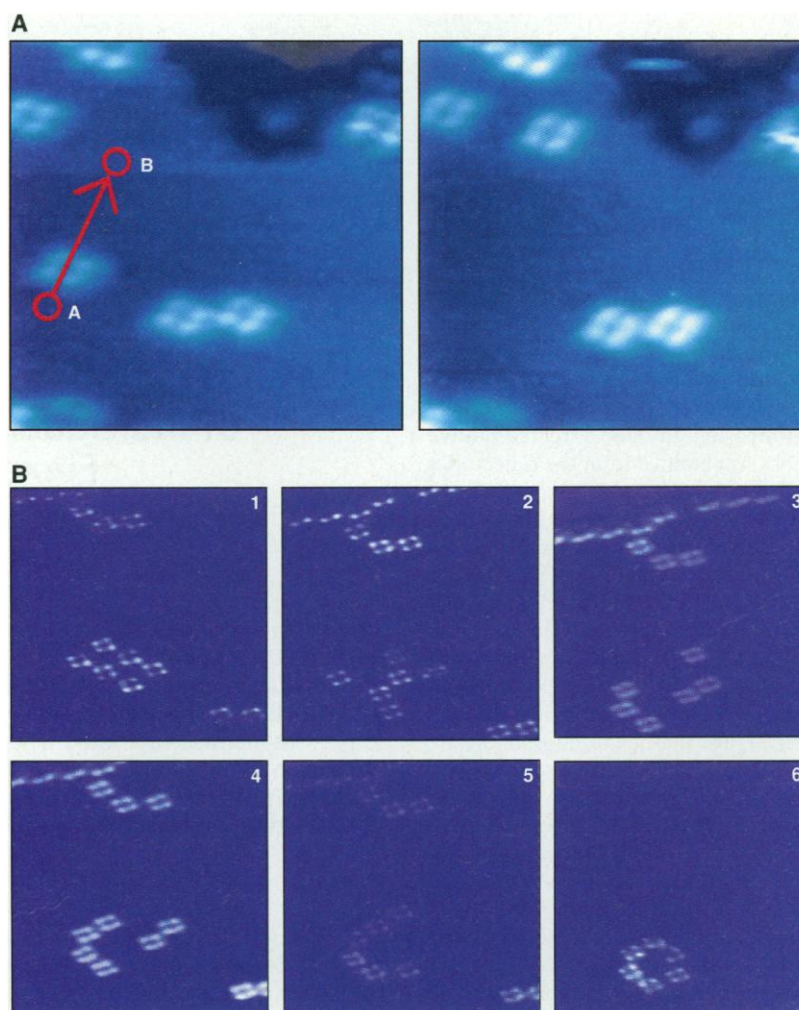


Fig. 3. (A) Movement of one individual molecule. In the left panel, the tip is positioned at point A, tunneling parameters are changed for movement, and the tip is moved to point B across the position of the previously imaged molecule. After a switch back to imaging mode, the scan shown in the right panel reveals a displacement of the molecule. The positions of all other molecules remain unaffected. (B) Six stages in the construction of a hexameric ring. First an as-grown array of six Cu-TBP molecules is disassembled. In the subsequent frames, each molecule is individually repositioned to form a hexagonal ring. The three clustered molecules at the top of the imaged frame (26 nm by 26 nm in size) remain unchanged during the entire series.

with the surface through a van der Waals interaction. For these studies, we selected a Cu(100) substrate, which offers the optimum adsorption characteristics of labile bonding with the *t*-butyl groups.

We used an ultrahigh-vacuum STM operating at room temperature (3) to characterize the orientation and internal molecular structure of the molecular overlayers. Atomically clean Cu(100) surfaces were exposed to 10 to 15% of a monolayer coverage of Cu-TBP-porphyrin followed by an annealing at 550 K. Subsequent STM characterization revealed nucleation of well-ordered islands (Fig. 2). Calculated STM images made with the STM electron-scattering quantum chemistry (STM-ESQC) technique (4) indicate that each of the four bright symmetric lobes seen in Fig. 2 corresponds to a DTP side group, which is in agreement with the calibrated dimensions of the image. This permits interpretation of the images in terms of orientation and the position of molecular "units."

A detailed analysis (5) of STM time-lapsed imaging sequences (6) under different imaging conditions allows two sets of

tunneling parameters to be identified (defined by tip voltage V_t and set current I_t) for either imaging or moving of individual molecules with the STM tip. The imaging mode occurred at high gap resistance ($R = 27.5$ gigohm), with $V_t \sim \pm 2200$ mV and $I_t \sim 80$ pA, whereas displacement was observed at low gap resistances ($R = 10$ to 15 megohm; $V_t \sim \pm 30$ mV and $I_t = 2$ to 3 nA). Manipulation software (7) allowed mouse-controllable, two-dimensional translations of the tip across the surface as well as switching between moving and imaging parameters.

Before a positioning sequence was started, a selected area of the sample was repeatedly imaged to ensure that no molecular motion occurred under the prevalent imaging conditions and that thermal drift was minimal. One molecule was then selected and displaced in a predefined direction (Fig. 3A). Such sequences can be combined so as to move a number of molecules to build up more complex patterns. To illustrate the principle (Fig. 3B), an island consisting of a two by three array was first disrupted by dragging the STM tip across it in the move-

ment mode. Then the molecules were individually rearranged to form a hexagonal ring. Such rings do not naturally form upon annealing of the molecule on the square lattice of Cu(100).

Analysis of the molecular displacement after lateral approach and retraction shows that repulsion between the tip and the molecule is responsible for the translation. The low resistance used, typically 10 megohm, suggests a "pushing" mechanism as proposed in preliminary manipulation experiments of C_{60} (8).

To understand the crucial role of the DTP side groups (legs) that contact the surface, we performed molecular mechanics simulations. The molecular geometry was optimized for molecules adsorbed on the Cu(100) surface in the presence of a tip. An adiabatic approximation was chosen to represent the long (~ 10 ms) time scales of the tip motion. Stages of the simulated positioning process are presented in Fig. 4A. When the tip laterally approached the TBP-porphyrin molecule (top), its molecular structure initially distorted as a result of the increase in repulsive force. This force increased until the potential well for lateral displacement was overcome (bottom).

The conditions for either scanning over a molecule in imaging mode or pushing it sideways depend on both the potential barrier for lateral displacement of the contacting *t*-butyl groups and the internal flexibility of the molecule, which reduces the effective molecular height in the junction. The force exerted on the molecule was calculated as a function of the relative positions of the Cu-TBP molecule and the tip at various tip-sample separations z (Fig. 4B). The molecule experienced only a slight increase in attractive force at $11 \text{ \AA} < z < 13 \text{ \AA}$. As we decreased the separation to $z = 9 \text{ \AA}$, this force increased significantly, with attractive and repulsive components peaking at ~ 1 and ~ 0.8 nN, respectively, as the tip was translated across the surface. The increase in force is associated with the interaction of the TBP side groups (height of $\sim 10 \text{ \AA}$) and the tip. Scanning at yet lower separations rapidly increased the calculated force and concomitantly increased the resistance to further molecular flexure. The crossover to lateral displacement occurred at $z < 8 \text{ \AA}$, which corresponds to a junction resistance of $R < 40$ megohm. This is in agreement with the experimental value of $R = 10$ megohm. For larger values, $z > 11 \text{ \AA}$, corresponding to the imaging mode resistance at $R > 2.6$ gigohm, the *t*-butyl groups were only slightly perturbed by the tip.

The forces exerted by the tip produce a substantial adjustment of the molecular conformation. This occurs primarily by ro-

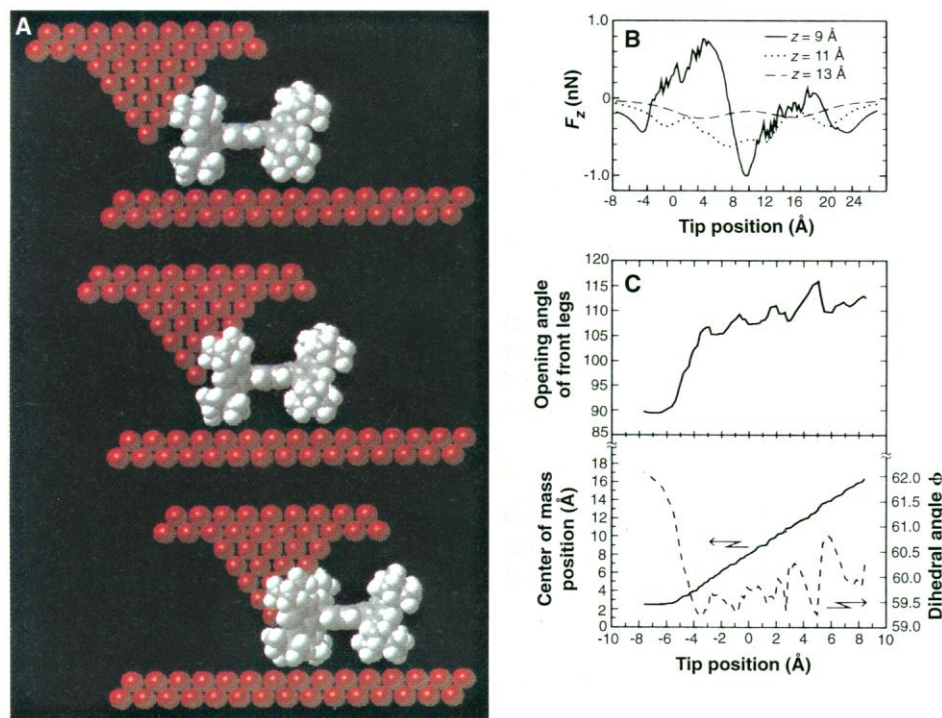


Fig. 4. (A) Selected snapshots of simulated movement with the use of the STM-ESQC molecular mechanics technique. Initially, the molecule lies relaxed next to the approaching tip (top). As the tip is moved laterally, the front legs open asymmetrically (center). After additional lateral steps, the molecule assumes a more relaxed conformation after moving (bottom). (B) Visualization of the crossover from squeezing of the molecule to lateral displacement. The force interaction (F_z) is plotted versus the tip displacement for different gap separations z . At 9 \AA , repulsive interaction between the TBP substituents and the tip sets in, which is in good agreement with experimental findings. (C) Lower panel: Displacement of the porphyrin molecule's Cu center atom (solid line) and rotation (dihedral) angle ϕ of one of the front TBP substituents (dashed line) as a function of tip displacement. The dihedral rotations of the two front legs are uncorrelated. Upper panel: Opening angle between the two front TBP substituents in the plane of the molecule. The out-of-phase discontinuity of the torsion angle results in the discontinuous displacement of the molecule.

tation of the TBP groups around the phenyl-porphyrin σ bond. In terms of the mechanics of motion, rotation of the rear TBP side groups is blocked by the tip, whereas the front TBP side groups show uncorrelated oscillatory lateral and torsional motions. The former effect produces an opening of the angle between the two front TBP groups from 90° to $\sim 115^\circ$ (Fig. 4C, top). The resulting translational motion resembles a “slip-stick”-type action of the individual TBP side groups with the surface (Fig. 4C, bottom). This uncorrelated slip-stick action of the individual legs effectively lowers the barrier for lateral displacement as compared with that of a rigid molecule—a crucial aspect of the nanomechanics of movement for this molecule. This mechanism is characteristically different from sliding processes used for low-temperature manipulation (9).

The control of internal molecular mechanics and of interactions between the molecule and the surface is a prerequisite for selective positioning and assembly. We have demonstrated that functional groups attached to a rigid planar molecule can

maintain thermally stable bonding, while being sufficiently labile to facilitate tip-induced translation without rupturing internal molecular bonds. We propose this conceptual approach of specific functionalization to separate substrate-molecular interactions as a step that goes beyond current approaches of engineering on the molecular scale.

REFERENCES AND NOTES

1. C. F. Quate, in *Highlights in Condensed Matter Physics and Future Prospects*, NATO ASI Series B (Plenum, New York, 1991), vol. 285, pp. 573–630; H. Rohrer, in *Nanosources and Manipulation of Atoms Under High Fields and Temperatures: Applications*, V. T. Binh *et al.*, Eds. (Kluwer, Dordrecht, 1993), vol. 235, pp. 1–12; J. A. Stroscio and D. M. Eigler, *Science* **254**, 1319 (1991).
2. D. M. Eigler and E. K. Schweizer, *Nature* **344**, 524 (1990); M. F. Crommie, C. P. Lutz, D. M. Eigler, *Science* **262**, 218 (1993); G. Meyer, B. Neu, K. H. Rieder, *Appl. Phys. A* **60**, 343 (1995).
3. R. Gaisch *et al.*, *Ultramicroscopy* **42–44**, 1621 (1992).
4. P. Sautet and C. Joachim, *Chem. Phys. Lett.* **185**, 23 (1991); *Surf. Sci.* **271**, 387 (1992); C. Chavy, C. Joachim, A. Altibelli, *Chem. Phys. Lett.* **214**, 569 (1993).
5. T. A. Jung, R. R. Schlittler, J. K. Gimzewski, unpublished data.

6. J. K. Gimzewski, R. Berndt, R. R. Schlittler, *Phys. Rev. B* **45**, 6844 (1992).
7. Manipulation software was developed in collaboration with M. E. Welland, M. Murrel, and T. Wong (University of Cambridge) under the European Union ESPRIT basic research project PRONANO (project number 8523).
8. J. K. Gimzewski, S. Modesti, T. David, R. R. Schlittler, *J. Vac. Sci. Technol. B* **12**, 1942 (1994); P. H. Beton, A. Dunn, P. Moriarty, *Appl. Phys. Lett.* **67**, 1075 (1995).
9. X. Bouju, C. Joachim, C. Girard, P. Sautet, *Phys. Rev. B* **47**, 7454 (1993); D. M. Eigler, C. P. Lutz, W. E. Rudge, *Nature* **352**, 600 (1991); R. E. Walkup, D. M. Newsom, P. Avouris, *Phys. Rev. B* **48**, 1858 (1993); N. D. Lang, *ibid.* **49**, 2067 (1994).
10. H. Song, C. A. Reed, W. R. Scheidt, *J. Am. Chem. Soc.* **111**, 6865 (1989); B. S. Erler, W. F. Scholz, Y. J. Lee, W. R. Scheidt, C. A. Reed, *ibid.* **109**, 2644 (1987); T. K. Miyamoto, N. Sugita, Y. Matsumoto, Y. Sasaki, M. Konno, *Chem. Lett. (Japan)* (1983), p. 1695.
11. We thank P. Guéret and H. Rohrer for enlightening and helpful discussions, M. E. Welland for valuable conversations, and T. Takami for providing the molecules used in this study. We gratefully acknowledge partial support by the Bundesamt für Bildung und Wissenschaft of Switzerland through the European Union ESPRIT basic research project PRONANO (8523). C.J. and H.T. thank the Région Midi-Pyrénées and the CNRS Groupement de Recherche NanoMips (1145) for financial support during this work.

29 September 1995; accepted 13 November 1995

The Shape of Mars and the Topographic Signature of the Hemispheric Dichotomy

David E. Smith and Maria T. Zuber

Reanalysis of occultation data from the Mariner 9 and Viking Orbiter spacecraft to determine the shape of Mars indicated that the hemispheric dichotomy is not a fundamental feature of the shape of the planet. It is a consequence of an approximately 3-kilometer offset between Mars's center of mass and center of figure, and the boundary, along most of its length, consists of broad, gradual surface slopes over distances of thousands of kilometers. This result was supported by analysis of high spatial resolution Earth-based radar topographic profiles. Any successful model for the origin of the dichotomy must explain a planet with an ellipsoidal shape and a long wavelength gradual topographic transition between the northern and southern hemispheres.

The surface of Mars is distinctly different in the northern and southern hemispheres. The south is old and heavily cratered, whereas the north is younger and lightly cratered and was probably volcanically resurfaced early in Mars's history (1, 2). This hemispheric dichotomy is characterized by a geologic boundary between the hemispheres that is expressed as knobby and fretted terrains and detached plateaus (2–4) distributed over a relatively limited width of ~ 700 km (5). Along the boundary, eleva-

tions have been interpreted to decrease from south to north by ~ 1 to 3 km (1, 6, 7), and the change in topography has been correlated with geologic features (8).

The formation of the dichotomy has been attributed to internal processes, such as postaccretionary core formation (9), and to crustal delamination (in the northern hemisphere) and underplating (in the southern hemisphere) by vigorous mantle convection (10). It has also been proposed that the low northern hemisphere was the result of a massive impact (5, 11) or impacts (12), and this region may have been the site of an early martian ocean (13). The lack of gravity anomalies along the boundary (14) may indicate thick crust beneath the southern highlands and thinner crust beneath the northern lowlands (1, 15).

In addition, the boundary region has been proposed as the site of relic plate boundaries (16). Consequently, understanding the origin of the hemispheric difference has implications for the evolution and internal structure of Mars.

Most analyses of the origin of the dichotomy have been based on global topographic models (8) with poor long-wavelength accuracy (17). The topography has also been studied by means of higher spatial resolution measurements derived from photogrammetry, stereo imaging, and ultraviolet spectra (7, 18). Although these methods yield information on relative heights within an individual image frame or mosaic, the heights cannot be placed in a global reference frame and are of limited utility in relating local structure to global structure.

Radio occultation measurements (19–22) provide estimates of the radius of the planet at the time (and location) when the radio signal from a spacecraft is lost (occulted) behind the planet or emerges from behind the planet in its orbit (23). Occultation data formed the basis of several early determinations of Mars's topography (21, 22, 24) and were included in more recent U.S. Geological Survey (USGS) digital elevation models (DEMs) (8), but the data have not been analyzed since the 1970s. Here, we reanalyzed these data by using improved spacecraft orbital information (25), the latest planetary ephemerides and dynamical information (26), and revised atmospheric refraction correc-

D. E. Smith, Laboratory for Terrestrial Physics, NASA/Goddard Space Flight Center, Greenbelt, MD 20771, USA.

M. T. Zuber, Department of Earth, Atmospheric and Planetary Sciences, Massachusetts Institute of Technology, Cambridge, MA 02139–4307, USA, and Laboratory for Terrestrial Physics, NASA/Goddard Space Flight Center, Greenbelt, MD 20771, USA.